ACS MATERIALS Au
AN OPEN ACCESS JOURNAL OF THE AMERICAN CHEMICAL SOCIETY

pubs.acs.org/materialsau Article

Photoactivation Properties of Self-n-Doped Perylene Diimides: Concentration-dependent Radical Anion and Dianion Formation

Daniel Powell, Zayn Rhodes, Xinwen Zhang, Edwin J. Miller, McKenzie Jonely, Kameron R. Hansen, Chideraa I. Nwachukwu, Andrew G. Roberts, He Wang, Rodrigo Noriega, Shelley D. Minteer, and Luisa Whittaker-Brooks*

Cite This: *ACS Mater. Au* 2022, 2, 482–488 Read Online

ACCESS | Metrics & More | Article Recommendations | Supporting Information

ABSTRACT: Perylene diimides (PDIs) have garnered attention as organic photocatalysts in recent years for their ability to drive challenging synthetic transformations, such as aryl halide reduction and olefin iodoperfluoroalkylation. Previous work in this area employs spectator pendant groups attached to the imide nitrogen positions of PDIs that are only added to impart solubility. In this work, we employ electron-rich ammonium iodide or ammonium hydroxide pendant groups capable of self-n-doping the PDI core to form radical anions ($\mathbf{R}^{\bullet-}$) and dianions ($\mathbf{D}^{\bullet\bullet 2-}$). We observe $\mathbf{R}^{\bullet-}$ formation is favored at low concentrations where aliphatic linkers are able to freely rotate, while $\mathbf{D}^{\bullet\bullet 2-}$ formation is favored at elevated concentrations likely due to Coulombic stabilization between adjacent chromophores in a similar manner to that of Kasha exciton stabilization. Cyclic voltammetric measurements are consistent with steric encumbrance increasing the Lewis basicity of anions through Coulombic destabilization. However, sterics also inhibit dianion formation by disrupting aggregation. Finally, femtosecond transient absorption measurements reveal that low wavelength excitation (400 nm) preferentially favors the excitation of $\mathbf{R}^{\bullet-}$ to the strongly reducing doublet excited state $^2[\mathbf{R}^{\bullet-}]^*$. In contrast, higher wavelength excitation (520 nm) favors the formation of the singlet excited state $^1[\mathbf{N}]^*$. These findings highlight the importance of dopant architecture, counterion selection, excitation wavelength, and concentration on $\mathbf{R}^{\bullet-}$ and $\mathbf{D}^{\bullet\bullet 2-}$ formation, which has substantial implications for future photocatalytic applications. We anticipate these findings will enable more efficient systems based on self-n-doped PDIs.

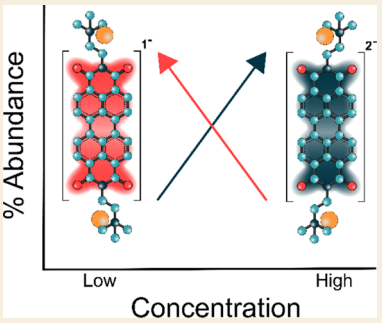

KEYWORDS: *self-doping, photodoping, concentration-dependent, radical anions, dianions, organic molecules*

INTRODUCTION

Perylene diimide (PDI) small organic molecules have become an increasingly relevant class of material in a broad range of applications beyond simple pigments, such as in biological systems, thermoelectrics, optoelectronics, sensing, photocatalysis, and synthetic photochemistry.[1−7] The successful utilization of PDIs in many of these applications requires an effective doping method to produce free carriers in the solid-state or radical anions in solution. For example, PDIs have garnered attention in synthetic photochemistry, such as aryl halide reduction and olefin iodoperfluoroalkylation, wherein the PDI is reduced by a sacrificial reductant under illumination to generate the radical anion $\mathbf{R}^{\bullet-}$.[8−14] $\mathbf{R}^{\bullet-}$ then absorbs another photon to produce the doublet excited state $^2[\mathbf{R}^{\bullet-}]^*$, which is a strong reducing agent capable of driving challenging reduction reactions.[14,15] Thus, the efficient production of $\mathbf{R}^{\bullet-}$ under irradiation is generally regarded as an essential step in PDI-based photocatalytic applications.

The method of covalently tethering two functionalities into the same catalytic system is an interesting prospect.[16] Self-n-doping is a method of electronic doping in organic semiconductors that has recently risen to prominence.[17] In the solid state, covalently incorporating amine/ammonium moieties into small molecules is an effective strategy to mitigate performance issues that arise from inhomogeneous dopant distribution.[18] Much of this work has focused on thermal activation of dopants,[19,20] with comparably less work on photoactivation in the solid-state or in solution.[21,22] Though underexplored, the method of self-doping could provide unique advantages to solution-based applications. The incorporation of self-doping ammonium salts to the PDI scaffold enhances solubility, and the doping process solely relies on the spatial organization of the molecular components as opposed to a diffusion-mediated process that relies on the shuttling of extrinsic reductants. This may prove to be of importance since it is known that anion reductants tend to form charge—transfer and anion—π interactions with the conjugated backbones of rylene dyes.[23] Moreover, substituents

Received: February 13, 2022
Revised: March 31, 2022
Accepted: April 8, 2022
Published: April 22, 2022

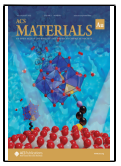

https://doi.org/10.1021/acsmaterialsau.2c00019
ACS Mater. Au 2022, 2, 482–488

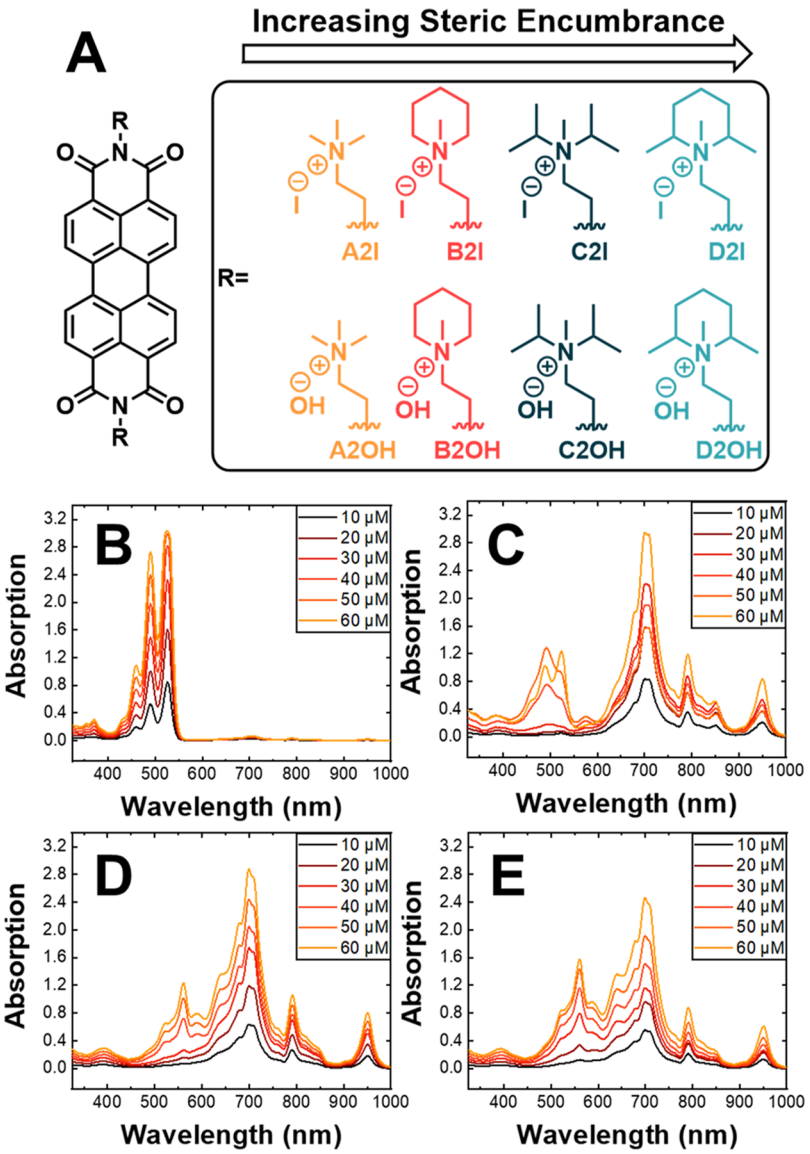

Figure 1. (A) Chemical structures of the self-doped PDIs investigated in this work. The naming scheme denotes the degree of steric encumbrance in alphabetical order, followed by the carbon chain length, and finally the counterion (e.g., **A2I**, **A2OH**, etc). (B) Absorption spectra of **A2I** measured in the dark and (C) after 90 min of irradiation with a 405 nm lamp. (D) Absorption spectra of **A2OH** measured in the dark and (E) after 90 min of irradiation with a 405 nm lamp. Sample concentrations are denoted in the legend.

added to the imide nitrogens are not critical to the performance of PDIs in photoelectrochemical transformations since these are not electrically connected to the PDI core where the anion radicals reside.[24] However, there is very little insight regarding the performance of self-dopants in solution, which is critical for future work. A detailed understanding of structure−function relationships in these systems is also critically lacking as acknowledged by the field[25] and serves as motivation to establish self-dopant design principles for new solution-based applications involving organic electronics.

RESULTS AND DISCUSSION

Here, we report the photoactivation of a series of progressively more sterically encumbered self-n-doped PDIs with iodide and hydroxide counterions, whose structures are shown in Figure 1A. The general naming scheme for this family of PDIs used throughout this work denotes the degree of steric encumbrance in alphabetical order, followed by the carbon spacer length, and counterion selection (e.g., **A2I**, **A2OH**, etc). All samples are soluble in water, dimethylformamide (DMF), and dimethyl sulfoxide (DMSO), and are moderately soluble in methanol and ethanol. For this work, samples were prepared and handled in the dark in 10−60 μM DMF solutions (details available in the Supporting Information). Figure 1B shows the absorption spectra of **A2I** solutions kept in the dark. The $S_0 \rightarrow S_1$ perylene core absorption band at 526 nm (0−0) is accompanied by Franck−Condon vibronic transitions 0−1 (490 nm), 0−2 (459 nm), and 0−3 (430 nm) that are characteristic of neutral PDI photoexcitation in solution (**N** → ^{1}[**N**]*). The peak ratio 0−0/0−1 is often used to measure the degree of aggregation, with higher values (∼1.7) being indicative of monodispersity and lower values (∼1) indicating H-type aggregation.[26] In all the iodide samples measured, the peak ratios decrease from ∼1.7 to 1 with increasing concentration due to interactions between neighboring perylene chromophores. Irradiation of **A2I** with a 405 nm

https://doi.org/10.1021/acsmaterialsau.2c00019
ACS Mater. Au 2022, 2, 482−488

lamp for 90 min induces a photochromic change from fluorescent orange to a dull green (Figure S1) due to an intramolecular self-n-doping process that forms $\mathbf{R}^{\bullet-}$, as shown in Figure 1C. $\mathbf{R}^{\bullet-}$ has six characteristic absorption peaks from ∼680 to 950 nm, with the 950 nm feature corresponding to the $D_0 \rightarrow D_1$ transition accompanied by a complex vibronic structure.[27] All samples bearing iodide counterions exhibit comparable behavior to **A2I** upon irradiation (Figures S2−S5). Samples with hydroxide counterions are strongly doped to the degree that **A2OH** includes a mixture of radical anions and dianions before any light exposure (Figure 1D). The singlet−singlet transitions of $\mathbf{D}^{\bullet\bullet 2-}$ are blueshifted from the doublet−doublet transitions of $\mathbf{R}^{\bullet-}$ and have five major peaks from ∼530−720 nm. Following photoexcitation, a portion of the radicals is converted to dianions, and the perylene core achieves a doping density up to approximately 130%, as shown in Figure 1E. The absorption spectra for all the compounds with hydroxide counterions are shown in Figures S6−S9. An immediately discernible feature is that **C2OH** and **D2OH** do not form dianions at all, and their presence is minimal in **B2OH** in the dark. Thus, steric encumbrance is found to slow or inhibit dianion formation in these systems. We also note that photoactivation of PDIs is also observed to a lesser degree in DMSO, though not at all in water where $\mathbf{R}^{\bullet-}$ species are immediately quenched.

Since the absorption characteristics of reduced PDIs are well defined, the relative components of **N**, $\mathbf{R}^{\bullet-}$, and $\mathbf{D}^{\bullet\bullet 2-}$ in each spectrum can be integrated and quantified in terms of their percentage abundance (Figure 2). However, spectral overlap between $\mathbf{R}^{\bullet-}$ and $\mathbf{D}^{\bullet\bullet 2-}$ requires fitting to evaluate abundances. The absorption spectra ($450\ \text{nm} < \lambda < 1000\ \text{nm}$) for each solution was fit, using linear regression, to a linear combination of $\mathbf{R}^{\bullet-}$ and $\mathbf{D}^{\bullet\bullet 2-}$ molar attenuation coefficient spectra, which have been reported previously in DMF.[27] Using Beer's law, the molar concentration of $\mathbf{R}^{\bullet-}$ and $\mathbf{D}^{\bullet\bullet 2-}$ were then computed for each solution. For the iodide samples, the concentration of $\mathbf{R}^{\bullet-}$ varies from 65−95% following irradiation, as shown in Figure 2A. The formation of $\mathbf{R}^{\bullet-}$ is favored in solutions of lower concentration (10−30 μM) both before and after irradiation, as well as during the overall radical conversion process (Figure S10). This trend is in stark contrast to the formation of dianions in the samples containing hydroxide counterions, which preferentially form in solutions of higher concentration both before and after irradiation (Figure 2B). To understand this trend, we first discuss the photoinduced electron transfer mechanism in PDIs.[28−30] In Figure 3, ground state **N** is photoexcited to $^1[\mathbf{N}]^*$, and $\mathbf{R}^{\bullet-}$ then forms when $^1[\mathbf{N}]^*$ is reductively quenched by the anion. The difference between this and previous reports is that, in the case of self-n-doping, the process is not diffusion-limited but instead mediated by chain rotation as the dopant folds back toward the imide acceptor moieties. Figure 4 offers a graphical representation of this concentration dependence of radical anion and dianion formation. At low concentrations (Figure 4A), chain rotation is relatively uninhibited, and doping proceeds readily. At elevated concentrations (Figure 4B), chain rotation is slowed by the presence of adjacent PDI structures. However, dianion formation is favored under these conditions, most likely due to a Coulombic stabilization effect that arises from electronic coupling between adjacent chromophores similar to that of exciton stabilization in Coulombically coupled PDI chromophores.[31,32] This view is supported by the fact that dianions do not form in the presence of tethered bulky dopants, which inhibit intermolecular attractions between adjacent chromophores. However, the precise arrangements of the various

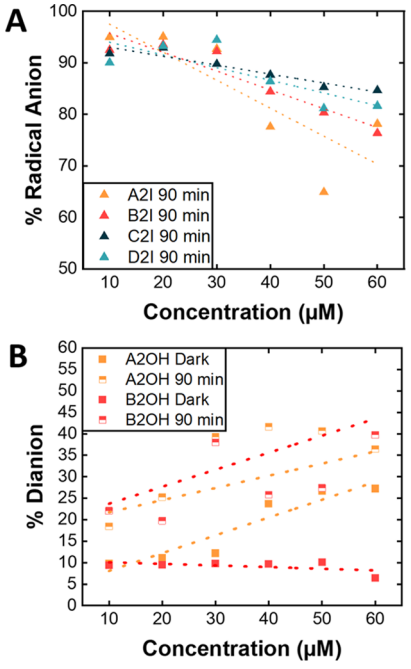

Figure 2. (A) Percentage radical anion abundance in iodide samples of varying concentration after 90 min of irradiation with a 405 nm lamp. (B) Percentage dianion abundance in **A2OH** and **B2OH** both before and after irradiation with a 405 nm lamp.

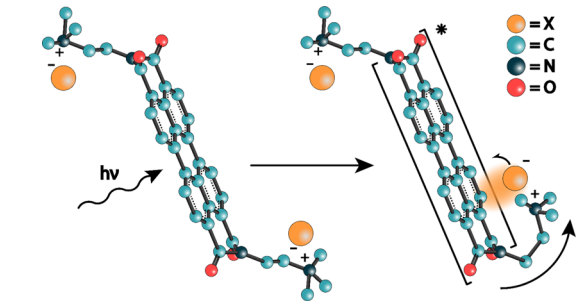

Figure 3. Graphical depiction of the doping mechanism. First, the neutral perylene core **N** is photoexcited to $^1[\mathbf{N}]^*$. The anion then transfers an electron to $^1[\mathbf{N}]^*$, thereby reducing it to generate $\mathbf{R}^{\bullet-}$.

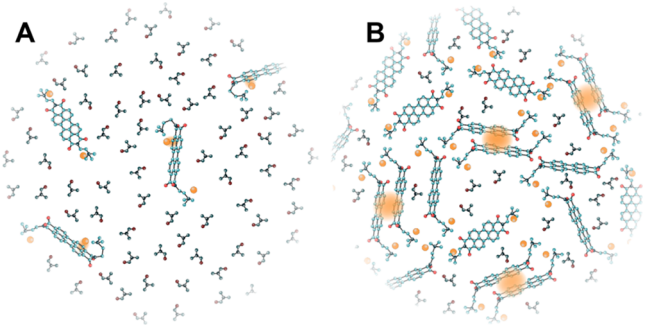

Figure 4. Graphical representations of concentration-dependent doping (A) in the low and (B) high concentration regimes.

https://doi.org/10.1021/acsmaterialsau.2c00019
ACS Mater. Au 2022, 2, 482−488

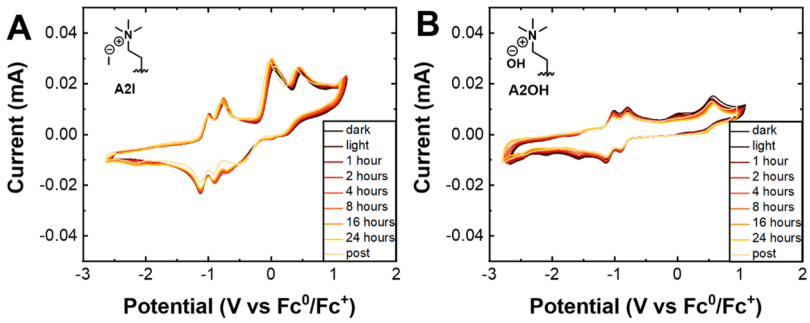

Figure 5. Cyclic voltammograms of (A) **A2I** and (B) **A2OH** in the dark and after various photoirradiation timepoints indicated in the legend. Each solution was measured at 10 μM in DMF and 100 mM tetrabutylammonium hexafluorophosphate ($TBAPF_6$) as a supporting electrolyte with ferrocene as an external standard reference potential, since a Ag/Ag^+ quasi-reference electrode was used. Scan rate: 100 mV/s.

components during dianion formation are yet to be determined.

To probe the limit of self-n-doping in solution, we irradiated samples for 24 h. We observe a dramatic decrease in the absorption intensity of the samples with iodide counterions (Figures S2–S5). While the features of **N** broaden, $\mathbf{R}^{\bullet-}$ is almost completely quenched, and a broad feature centered at ∼700 nm persists, which we assign to a charge-transfer state between iodide counterions and the PDI core.[23] In the samples with hydroxide counterions, we observe dianion quenching, and the spectrum of $\mathbf{R}^{\bullet-}$ slightly broadens (Figures S6–S9). Thus, all samples are prone to photodegradation due to the strongly reducing character of $^2[\mathbf{R}^{\bullet-}]^*$ and $\mathbf{D}^{\bullet\bullet 2-}$. The samples with hydroxide counterions degrade more slowly. A comparison of photocatalytic activity between both sample types could provide insight into the disputed catalytic mechanism of 4′-bromoacetophenone reduction.[33] We also observe that particles begin to precipitate at these longer timescales (Figure S11), and Mie scattering off of these particles contributes to spectral broadening.

Self-doped PDIs exhibit electrochromic color changes in response to changing oxidation state via cyclic voltammetry (CV).[34] Cyclic voltammograms were produced for each compound by first measuring in the dark and then scanning each hour during photoirradiation for 24 h. Voltammograms of **A2I** and **A2OH** are presented in Figure 5A,B, respectively. As the carboximide core substituents are electron-poor, PDIs generally share two reversible reduction waves at ∼−0.9 and −1.1 V versus ferrocene/ferrocenium (Fc^0/Fc^+) attributed to $\mathbf{R}^{\bullet-}$ and $\mathbf{D}^{\bullet\bullet 2-}$, respectively.[35] Incorporating two iodide counterions (Figure 5A) results in an I^-/I_2 redox process that occurs in two steps[36]

$$3I^- \rightleftharpoons I_3^- + 2e^- \quad (1)$$

$$I_3^- \rightleftharpoons \frac{3}{2}I_2 + e^- \quad (2)$$

These are at roughly twice the intensity of the oxidation waves for the perylene core due to the improved solubility of iodide versus hydroxide counterions. The irreversible reduction wave observed at −2.2 V versus Fc^0/Fc^+ is related to the photodoping process as it only appears and becomes more intense after doping (Figures S12–S14). This could be a reducible photodegradation product or the product of a complex reaction between triiodide, which forms as a product of photoactivated doping and **A2I**. The precise nature of this peak is unclear but may be related to the particles that begin to crash out of the solution over time. The first iodide oxidation also shifts and becomes more electronegative in sterically encumbered samples, **C2I** and **D2I**, which we attribute to the weaker ion-pairing between ammonium and iodide, making them better electron donors. The iodide counterions in **C2I** and **D2I** thus act as stronger Lewis bases, but steric encumbrance also prevents aggregation, which is important for a high degree of doping. The voltammograms for the samples with hydroxide counterions are more challenging to interpret (Figure 5B and S15–S17). As shown in the voltammograms, two quasi-reversible oxidation waves are observed, which we attribute to

$$2OH^- \rightleftharpoons H_2O_2 + 2e^- \quad (3)$$

$$H_2O_2 + 2OH^- \rightleftharpoons O_2 + 2H_2O + 2e^- \quad (4)$$

The two reversible reduction waves at ∼−1.5 and −2 V versus Fc^0/Fc^+ are more challenging to assign, though they are related to electronic doping, similar to the iodide counterion samples. For example, the peak currents of the −2 V versus Fc^0/Fc^+ feature are relatively larger in **A2OH** and **B2OH**, which form dianions, and virtually non-existent in **C2OH** and **D2OH**, which do not. These peaks could arise from a photodegradation product, though we contend this is unlikely given that the observed peaks are generally more pronounced in the dark than after irradiation. Instead, we attribute these peaks to the reduction of H_2O_2 and O_2.

We also investigated the absorption and luminescence behavior of our PDI series using both femtosecond transient absorption (TA) and time-resolved photoluminescence (TRPL) spectroscopies. TA was used to probe whether the photophysical properties of the perylene core were altered by the presence of the dopant moieties. Additionally, both $\mathbf{R}^{\bullet-}$ and $\mathbf{D}^{\bullet\bullet 2-}$ are non-luminescent due to non-radiative relaxation, and thus total fluorescence and TRPL were used to probe **N** and $^1[\mathbf{N}]^*$, respectively. TA of PDIs generally involve an $S_0 \rightarrow S_1$ ground-state photobleach of **N**, often accompanied by stimulated emission, concomitant with the growth of the excited singlet state $^1[\mathbf{N}]^*$ photoinduced absorption transient $S_1 \rightarrow S_n$ ($n > 1$), and $^1[\mathbf{N}]^*$ quickly relaxes (within a few ns) back to the ground state **N**. The absorption of $\mathbf{R}^{\bullet-}$ and $^1[\mathbf{N}]^*$ appear in the same spectral region due to the fact that both excitations occur at similar energies, both involve the LUMO of **N**, and the energy of the LUMO is not dramatically altered when populated by an electron.[27] TA maps and spectra of iodide samples excited at 400 nm are shown in Figures S18–S21. Photobleaching occurs at 490–540 nm accompanied by stimulated emission at 560 nm and a photoinduced absorption feature centered at 700 nm, which decays after 7 ns. The

https://doi.org/10.1021/acsmaterialsau.2c00019
ACS Mater. Au 2022, 2, 482–488

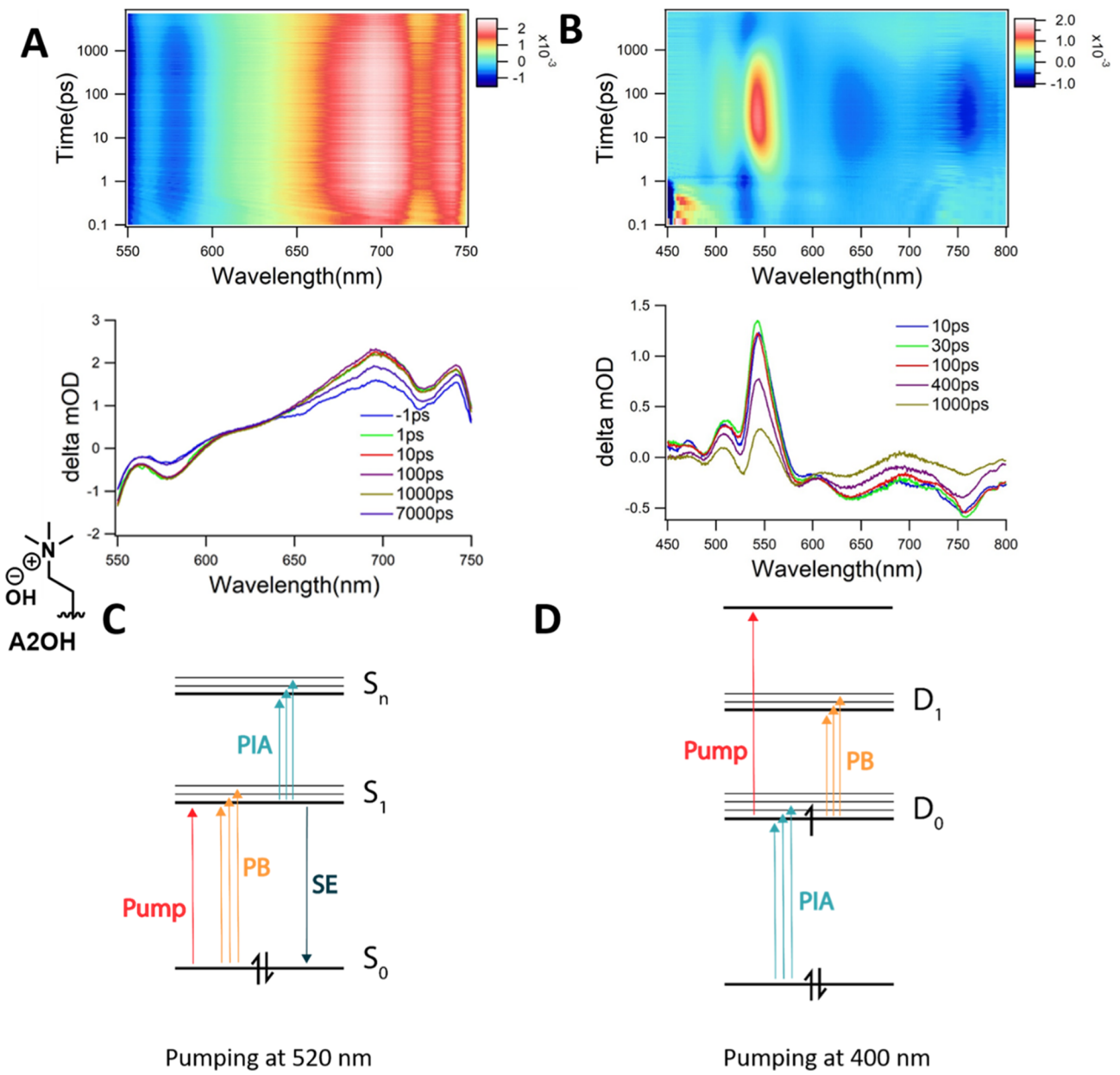

Figure 6. (A) Femtosecond transient absorption maps and spectra for **A2OH** pumped at 520 nm and (B) 400 nm and were not exposed to any other light sources. (C) Energy level diagrams depicting the two pathways activated by the different excitation wavelengths. Pumping at 520 nm (left) bleaches the $S_0 \rightarrow S_1$ transition of **N** accompanied by stimulated emission and a $S_1 \rightarrow S_n$ absorption transient of $^1[\mathbf{N}]^*$ centered at 700 nm. In contrast, pumping at 400 nm (right) bleaches the $D_0 \rightarrow D_1$ transition of $\mathbf{R}^{\bullet-}$ and is accompanied by the transient absorption of the ground-state excitation.

overall intensity of these features progressively decreases after irradiation, and the total fluorescence brightness also decreases (Table S1) as **N** is converted to $\mathbf{R}^{\bullet-}$. The fluorescence lifetimes also vary slightly after irradiation due to aggregate formation among the remaining neutral PDIs, which can be observed in the 0−0/0−1 peak ratios of the **N** absorption bands (Figures S2−S5). Contrastingly, the TA maps of **A2OH** depend on the excitation wavelength. When the sample is excited at 520 nm near the ground-state absorption energy, **N** photobleaches and $^1[\mathbf{N}]^*$ rises in the same manner as iodide samples, as shown in Figure 6A. The overall TA intensity is quite low, which is unsurprising given the low concentration of **N** in **A2OH**, as evidenced by the total measurable fluorescence (Table S2). Interestingly, when the same sample is excited at 400 nm, the features are inverted, as shown in Figure 6B. At this excitation wavelength, $\mathbf{R}^{\bullet-}$ is preferentially excited to $^2[\mathbf{R}^{\bullet-}]^*$, and **N** is excited to $^1[\mathbf{N}]^*$. Electronic diagrams for each of these pathways are illustrated in Figure 6C,D. These findings demonstrate that $^2[\mathbf{R}^{\bullet-}]^*$ can be preferentially selected at lower excitation wavelengths, which is an important finding for future photocatalytic work.

CONCLUSIONS

In summary, we have presented a series of soluble self-n-doped perylene diimides with increasingly sterically encumbered dopant moieties for use in photocatalytic applications. Anion doping proceeds readily when samples dissolved in DMF are excited with a 405 nm lamp, achieving anywhere from ∼65−

https://doi.org/10.1021/acsmaterialsau.2c00019
ACS Mater. Au 2022, 2, 482−488

130% doping depending on counterion selection. Anion doping generally follows Lewis basicity strength, with hydroxide being the stronger dopant. We observed radical anion formation is favored at low concentrations where associated ion pairs move more freely, but dianion formation is favored at high concentrations due to the stabilizing interactions of adjacent chromophores. Additionally, while steric encumbrance was found to increase the Lewis base strength of the anions by weakening counterion interactions, sterics also disrupt aggregation, which is essential for dianion formation. Finally, we found irradiation wavelength drives $\mathbf{R}^{\bullet-}$ excitation; lower wavelengths far from the ground-state absorption band promote the formation of $^2[\mathbf{R}^{\bullet-}]^*$, which helps to explain why these excitation wavelengths are able to drive synthetic transformations. Future work to establish the catalytic ability of self-n-doped PDIs is forthcoming and more groundwork to promote the synthetic modulation of organic materials to maximize their doping efficiency is needed. Specifically, the use of divalent anions may drive forward reactions more efficiently than monovalent anions due to their improved electron-donating ability.[37]

■ ASSOCIATED CONTENT

Supporting Information

The Supporting Information is available free of charge at https://pubs.acs.org/doi/10.1021/acsmaterialsau.2c00019.

Experimental methods, synthesis and photoactivation of all self-n-doped PDIs with different iodide and hydroxide counterions, absorption studies, cyclic voltammetry, transient absorption, and time-resolved photoluminescence data (PDF)

■ AUTHOR INFORMATION

Corresponding Author

Luisa Whittaker-Brooks − *Department of Chemistry, University of Utah, Salt Lake City, Utah 84112, United States;* orcid.org/0000-0002-1130-1306; Email: luisa.whittaker@utah.edu

Authors

Daniel Powell − *Department of Chemistry, University of Utah, Salt Lake City, Utah 84112, United States*

Zayn Rhodes − *Department of Chemistry, University of Utah, Salt Lake City, Utah 84112, United States*

Xinwen Zhang − *Department of Physics, University of Miami, Coral Gables, Florida 33146, United States*

Edwin J. Miller − *Department of Chemistry, University of Utah, Salt Lake City, Utah 84112, United States*

McKenzie Jonely − *Department of Chemistry, University of Utah, Salt Lake City, Utah 84112, United States*

Kameron R. Hansen − *Department of Chemistry, University of Utah, Salt Lake City, Utah 84112, United States*

Chideraa I. Nwachukwu − *Department of Chemistry, University of Utah, Salt Lake City, Utah 84112, United States;* orcid.org/0000-0002-9143-3228

Andrew G. Roberts − *Department of Chemistry, University of Utah, Salt Lake City, Utah 84112, United States;* orcid.org/0000-0002-2221-534X

He Wang − *Department of Physics, University of Miami, Coral Gables, Florida 33146, United States;* orcid.org/0000-0003-1365-0304

Rodrigo Noriega − *Department of Chemistry, University of Utah, Salt Lake City, Utah 84112, United States;* orcid.org/0000-0003-1199-0866

Shelley D. Minteer − *Department of Chemistry, University of Utah, Salt Lake City, Utah 84112, United States;* orcid.org/0000-0002-5788-2249

Complete contact information is available at: https://pubs.acs.org/10.1021/acsmaterialsau.2c00019

Author Contributions

This manuscript was written through the contributions of all authors. All authors have given approval to the final version of the manuscript.

Notes

The authors declare no competing financial interest.

■ ACKNOWLEDGMENTS

This work was supported by the NSF under award # DMR 1824263. EPR studies were supported by the NSF under award # CBET 2016191. L.W.B. would also like to acknowledge the financial support from the Sloan Foundation and the Dreyfus Foundation. X.Z. and H.W. acknowledge the financial support by the Air Force Office of Scientific Research (AFOSR) award FA9550-17-1-0099.

■ REFERENCES

(1) Zhang, F.; Li, W.; Jiang, T.; Li, X.; Shao, Y.; Ma, Y.; Wu, J. Real Roles of Perylene Diimides for Improving Photocatalytic Activity. *RSC Adv.* **2020**, *10*, 23024−23037.

(2) Wu, G.; Zhang, Z.-G.; Li, Y.; Gao, C.; Wang, X.; Chen, G. Exploring High-Performance N-Type Thermoelectric Composites Using Amino- Substituted Rylene Dimides and Carbon Nanotubes. *ACS Nano* **2017**, *11*, 5746−5752.

(3) Wang, Z.; Zheng, N.; Zhang, W.; Yan, H.; Xie, Z.; Ma, Y.; Huang, F.; Cao, Y. Self-Doped, n-Type Perylene Diimide Derivatives as Electron Transporting Layers for High-Efficiency Polymer Solar Cells. *Adv. Energy Mater.* **2017**, *7*, 1700232.

(4) Che, Y.; Yang, X.; Liu, G.; Yu, C.; Ji, H.; Zuo, J.; Zhao, J.; Zang, L. Ultrathin N-Type Organic Nanoribbons with High Photoconductivity and Application in Optoelectronic Vapor Sensing of Explosives. *J. Am. Chem. Soc.* **2010**, *132*, 5743−5750.

(5) Ronconi, F.; Syrgiannis, Z.; Bonasera, A.; Prato, M.; Argazzi, R.; Caramori, S.; Cristino, V.; Bignozzi, C. A. Modification of Nanocrystalline WO_3 with a Dicationic Perylene Bisimide: Applications to Molecular Level Solar Water Splitting. *J. Am. Chem. Soc.* **2015**, *137*, 4630−4633.

(6) Bonchio, M.; Syrgiannis, Z.; Burian, M.; Marino, N.; Pizzolato, E.; Dirian, K.; Rigodanza, F.; Volpato, G. A.; la Ganga, G.; Demitri, N.; Berardi, S.; Amenitsch, H.; Guldi, D. M.; Caramori, S.; Bignozzi, C. A.; Sartorel, A.; Prato, M. Hierarchical Organization of Perylene Bisimides and Polyoxometalates for Photo-Assisted Water Oxidation. *Nat. Chem.* **2019**, *11*, 146−153.

(7) Takada, T.; Ido, M.; Ashida, A.; Nakamura, M.; Fujitsuka, M.; Kawai, K.; Majima, T.; Yamana, K. Photocurrent Generation through Charge-Transfer Processes in Noncovalent Perylenediimide/DNA Complexes. *Chem.—Eur J.* **2015**, *21*, 6846−6851.

(8) Ghosh, I.; Ghosh, T.; Bardagi, J. I.; König, B. Reduction of Aryl Halides by Consecutive Visible Light-Induced Electron Transfer Process. *Science* **2014**, *346*, 725−728.

(9) Rosso, C.; Filippini, G.; Cozzi, P. G.; Gualandi, A.; Prato, M. Highly Performing Iodoperfluoroalkylation of Alkenes Triggered by the Photochemical Activity of Perylene Diimides. *ChemPhotoChem* **2019**, *3*, 193−197.

(10) Wang, C.-S.; Dixneuf, P. H.; Soulé, J.-F. Photoredox Catalysis for Building C-C Bonds from C(sp^2)-H Bonds. *Chem. Rev.* **2018**, *118*, 7532−7585.
(11) Rosso, C.; Filippini, G.; Prato, M. Use of Perylene Diimides in Synthetic Photochemistry. *Eur. J. Org. Chem.* **2021**, *2021*, 1193−1200.
(12) Glaser, F.; Kerzig, C.; Wenger, O. S. Multi-Photon Excitation in Photoredox Catalysis: Concepts, Applications, Methods. *Angew. Chem., Int. Ed.* **2020**, *59*, 10266.
(13) Romero, N. A.; Nicewicz, D. A. Organic Photoredox Catalysis. *Chem. Rev.* **2016**, *116*, 10075−10166.
(14) Zeng, L.; Liu, T.; He, C.; Shi, D.; Zhang, F.; Duan, C. Organized Aggregation Makes Insoluble Perylene Diimide Efficient for the Reduction of Aryl Halides via Consecutive Visible Light-Induced Electron-Transfer Processes. *J. Am. Chem. Soc.* **2016**, *138*, 3958−3961.
(15) Zeman, C. J.; Kim, S.; Zhang, F.; Schanze, K. S. Direct Observation of the Reduction of Aryl Halides by a Photoexcited Perylene Diimide Radical Anion. *J. Am. Chem. Soc.* **2020**, *142*, 2204−2207.
(16) Zhang, Z.; Smal, V.; Retailleau, P.; Voituriez, A.; Frison, G.; Marinetti, A.; Guinchard, X. Tethered Counterion-Directed Catalysis: Merging the Chiral Ion-Pairing and Bifunctional Ligand Strategies in Enantioselective Gold(I) Catalysis. *J. Am. Chem. Soc.* **2020**, *142*, 3797−3805.
(17) Russ, B.; Robb, M. J.; Popere, B. C.; Perry, E. E.; Mai, C.-K.; Fronk, S. L.; Patel, S. N.; Mates, T. E.; Bazan, G. C.; Urban, J. J.; Chabinyc, M. L.; Hawker, C. J.; Segalman, R. A. Tethered Tertiary Amines as Solid-State n-Type Dopants for Solution-Processable Organic Semiconductors. *Chem. Sci.* **2016**, *7*, 1914−1919.
(18) Powell, D.; Campbell, E. v.; Flannery, L.; Ogle, J.; Soss, S. E.; Whittaker-Brooks, L. Steric Hindrance Dependence on the Spin and Morphology Properties of Highly Oriented Self-Doped Organic Small Molecule Thin Films. *Adv. Mater.* **2021**, *2*, 356−365.
(19) Reilly, T. H.; Hains, A. W.; Chen, H.-Y.; Gregg, B. A. A Self-Doping, O_2-Stable, n-Type Interfacial Layer for Organic Electronics. *Adv. Energy Mater.* **2012**, *2*, 455−460.
(20) Russ, B.; Robb, M. J.; Brunetti, F. G.; Miller, P. L.; Perry, E. E.; Patel, S. N.; Ho, V.; Chang, W. B.; Urban, J. J.; Chabinyc, M. L.; Hawker, C. J.; Segalman, R. A. Power Factor Enhancement in Solution-Processed Organic n-Type Thermoelectrics through Molecular Design. *Adv. Mater.* **2014**, *26*, 3473−3477.
(21) Matsunaga, Y.; Goto, K.; Kubono, K.; Sako, K.; Shinmyozu, T. Photoinduced Color Change and Photomechanical Effect of Naphthalene Diimides Bearing Alkylamine Moieties in the Solid State. *Chem. Eur J.* **2014**, *20*, 7309−7316.
(22) Han, D.; Han, J.; Huo, S.; Qu, Z.; Jiao, T.; Liu, M.; Duan, P. Proton Triggered Circularly Polarized Luminescence in Orthogonal- and Co-Assemblies of Chiral Gelators with Achiral Perylene Bisimide. *Chem. Commun.* **2018**, *54*, 5630−5633.
(23) Guha, S.; Goodson, F. S.; Corson, L. J.; Saha, S. Boundaries of Anion/Naphthalenediimide Interactions: From Anion-π Interactions to Anion-Induced Charge-Transfer and Electron-Transfer Phenomena. *J. Am. Chem. Soc.* **2012**, *134*, 13679−13691.
(24) Würthner, F.; Saha-möller, C. R.; Fimmel, B.; Ogi, S.; Leowanawat, P.; Schmidt, D. Perylene Bisimide Dye Assemblies as Archetype Functional Supramolecular Materials. *Chem. Rev.* **2016**, *116*, 962−1052.
(25) Scaccabarozzi, A. D.; Basu, A.; Aniés, F.; Liu, J.; Zapata-Arteaga, O.; Warren, R.; Firdaus, Y.; Nugraha, M. I.; Lin, Y.; Campoy-Quiles, M.; Koch, N.; Müller, C.; Tsetseris, L.; Heeney, M.; Anthopoulos, T. D. Doping Approaches for Organic Semiconductors. *Chem. Rev.* **2021**, *122*, 4420−4492.
(26) Hestand, N. J.; Spano, F. C. Expanded Theory of H- and J -Molecular Aggregates: The Effects of Vibronic Coupling and Intermolecular Charge Transfer. *Chem. Rev.* **2018**, *118*, 7069−7163.
(27) Gosztola, D.; Niemczyk, M. P.; Svec, W.; Lukas, A. S.; Wasielewski, M. R. Excited Doublet States of Electrochemically Generated Aromatic Imide and Diimide Radical Anions. *J. Phys. Chem. A* **2000**, *104*, 6545−6551.
(28) Takada, T.; Ashida, A.; Nakamura, M.; Fujitsuka, M.; Majima, T.; Yamana, K. Photocurrent Generation Enhanced by Charge Delocalization over Stacked Perylenediimide Chromophores Assembled within DNA. *J. Am. Chem. Soc.* **2014**, *136*, 6814−6817.
(29) Tauber, M. J.; Kelley, R. F.; Giaimo, J. M.; Rybtchinski, B.; Wasielewski, M. R. Electron Hopping in π-Stacked Covalent and Self-Assembled Perylene Diimides Observed by ENDOR Spectroscopy. *J. Am. Chem. Soc.* **2006**, *128*, 1782−1783.
(30) Giaimo, J. M.; Gusev, A. v.; Wasielewski, M. R. Excited-State Symmetry Breaking in Cofacial and Linear Dimers of a Green Perylenediimide Chlorophyll Analogue Leading to Ultrafast Charge Separation. *J. Am. Chem. Soc.* **2002**, *124*, 8530−8531.
(31) Kasha, M. Energy Transfer Mechanisms and the Molecular Exciton Model for Molecular Aggregates. *Radiat. Res.* **1963**, *20*, 55−70.
(32) Hestand, N. J.; Spano, F. C. Molecular Aggregate Photophysics beyond the Kasha Model: Novel Design Principles for Organic Materials. *Acc. Chem. Res.* **2017**, *50*, 341−350.
(33) Marchini, M.; Gualandi, A.; Mengozzi, L.; Franchi, P.; Lucarini, M.; Cozzi, P. G.; Balzani, V.; Ceroni, P. Mechanistic Insights into Two-Photon-Driven Photocatalysis in Organic Synthesis. *Phys. Chem. Chem. Phys.* **2018**, *20*, 8071−8076.
(34) Yang, L.; Wang, M.; Slattum, P. M.; Bunes, B. R.; Wang, Y.; Wang, C.; Zang, L. Donor-Acceptor Supramolecular Organic Nanofibers as Visible-Light Photoelectrocatalysts for Hydrogen Production. *ACS Appl. Mater. Interfaces* **2018**, *10*, 19764−19772.
(35) Lee, S. K.; Zu, Y.; Herrmann, A.; Geerts, Y.; Müllen, K.; Bard, A. J. Electrochemistry, Spectroscopy and Electrogenerated Chemiluminescence of Perylene, Terrylene, and Quaterrylene Diimides in Aprotic Solution. *J. Am. Chem. Soc.* **1999**, *121*, 3513−3520.
(36) Bentley, C. L.; Bond, A. M.; Hollenkamp, A. F.; Mahon, P. J.; Zhang, J. Voltammetric Determination of the Iodide/Iodine Formal Potential and Triiodide Stability Constant in Conventional and Ionic Liquid Media. *J. Phys. Chem. C* **2015**, *119*, 22392−22403.
(37) Tang, C. G.; Syafiqah, M. N.; Koh, Q.-M.; Zhao, C.; Zaini, J.; Seah, Q.-J.; Cass, M. J.; Humphries, M. J.; Grizzi, I.; Burroughes, J. H.; Png, R.-Q.; Chua, L.-L.; Ho, P. K. H. Multivalent Anions as Universal Latent Electron Donors. *Nature* **2019**, *573*, 519−525.

https://doi.org/10.1021/acsmaterialsau.2c00019
ACS Mater. Au 2022, 2, 482−488